5 Summary and Outlook

5.1 Summary

This work presents photoemission measurements of liquid water and aqueous salt solutions. A specially designed liquid microjet, providing a free liquid surface in vacuum, enables the detection of photoelectrons from highly volatile liquid surfaces. In combination with high-intensity synchrotron light from an undulator (U125 at BESSY II) for photoexcitation, in the 30 - 140 eV range, electron binding energies of the liquid constituents have been determined. Energies were obtained for liquid water's valence orbitals as well as for a number of solvated ions, particularly alkali cations and halide anions. Liquid water's electron binding energies are shifted to lower values as compared to the gas-phase by about 1.4 eV. This gas-liquid energy shift is accompanied by considerable peak broadening of the photoemission features. Both of this changes, however, vary by different amount for each orbital, which is assigned to the effect of hydrogen bonding (H-bonding) on water's electronic structure. The $1b_1$ derived valence band center is located 11.16 eV below vacuum, and has a width at half maximum of 1.45 eV. The binding energies of the subsequent valence orbitals, $3a_1$, $1b_2$, and $2a_1$ are 13.50, 17.34, and 30.90 eV, respectively. Largest peak widths, ca. 2.52 and 3.30 eV, are observed for the a_1 - symmetry orbitals $3a_1$ and $2a_1$, respectively.

One difficulty in quantitatively interpreting the peak position and width of pure liquid water (in terms of trends predicted by theory; see below) arises from the fact that one has to account for the existence of the liquid/vacuum interface. Oriented surface water molecules will give rise to a surface potential, which is expected to be small but not negligible, on the order of 20 - 80 meV. The precise value has not yet been determined. This missing information clearly complicates the interpretation of the present data. Moreover, electronic screening of the photoionized species by surrounding solvent molecules, as the photoelectron leaves the site, may also lead to spectral shifts on the order of ca. 1 - 2 eV. To summarize this part, the quantitative interpretation of experimental electron binding energies (but also

peak widths) of pure water, in terms of the influence of H-bonding on the molecular orbital structure, must await a more detailed understanding of liquid water's surface potential as well as of photoemission final state effects. Yet, experimental energy shifts can be reasonably well described within a simple dielectric continuum model (Born model).

More favorable in terms of identifying electronic structural differences between liquid and gas-phase were measurements of the relative partial photoionization cross sections, σ_i, of the water orbitals. Using 60, 80, and 100 eV photons, it could be shown that for the liquid the relative intensities of the $3a_1$ and $1b_2$ orbitals are considerably decreased. The drop of the latter intensity is argued to be associated with the electronic molecular orbital change due to H-bonding, and can be interpreted in terms of the variation of the respective anisotropy parameter β_{1b_2}. Notice that the $1b_2$ orbital is directed along the O-H axes. Furthermore, at least in the gas phase, this orbital has the lowest β value, which makes changes of this quantity particularly sensitive in the present experiment. The $3a_1$ intensity decrease, on the other hand, does not correlate with a significant change of the photoemission peak area, as this is only an apparent signal decrease accompanied by substantial peak broadening. In fact the $3a_1$ feature seems to be split into two components, which may be due to Davydov splitting. Hence the $3a_1$ signal drop is not associated with a change of σ_{3a_1}. This behavior parallels the importance of the $3a_1$ orbital in water binding to solid surfaces, suggesting that there is a certain analogy also for water bonding in H-bonding. Notice that both the water $3a_1$ [1] and the $1b_2$ [3] orbitals are expected to lose their original character in the presence of H-bonding. In the liquid phase the electronic charge is computed to be more spherically distributed around the oxygen atoms than in the gas phase.

A final observation regarding pure liquid water is the identification of photoelectron energy losses, which seem to correlate with energy loss function features as obtained by inelastic X-ray scattering. The effect is most noticeable in the photoemission spectra for ca. 50 eV electron binding energy, and can be ascribed to 18 eV - energy losses of photoelectrons initially originating from the water $2a_1$ orbital.

Systematic photoemission studies were performed for a number of aqueous salt solutions (XY for X = Li, Na, K, Cs, and Y = Cl, Br, I; CaI_2; $MgCl_2$; Na_2CO_3; $Na_4[Fe(CN)_6]$; $K_4[Fe(CN)_6]$; $K_3[Fe(CN)_6]$; But_4NI; $Prop_4NI$) in order to obtain information on electronic and structural details of ionic solvation by water molecules. Within the limits of the experiment (30 meV) no electron binding energy differences could be observed for a given solvated anion or cation, at least for the non-surface-active salts studied, as a function of the counter ion and even of the salt concentration. Hence, solvation shell structures are concluded to

barely change for the conditions mentioned, and binding energy changes must be well within the width of the peaks. Typical peak widths of aqueous ionic photoemission features are on the order of 1 eV, which is likely to reflect the existence of a distribution of solvation structures having slightly different energies. Also electronic structural differences for solvate (both anion and cation solvation) vs. bulk water are indistinguishable. Electron binding energy shifts with respect to the gas-phase ion are considerably different for solvated cations and anions. Solvated alkali ions exhibit solvation energy shifts up to 16 eV towards lower binding energies (e.g. from 47 to 35 eV for $Na^+(2p)$), while the halide anion energy shifts are smaller and in the opposite direction (e.g. from 3.6 to 9.6 eV for $Cl^-(3p)$). These differences can be explained by suitably applying the Born model to the photoemission process. This procedure is discussed in some detail here since it gives an interesting insight into the classical dielectric continuum model and its limits. Clearly, the understanding of the microscopic processes governing solvation requires a detailed knowledge of not only the water-ion but also the water-water interactions. The importance of cluster studies in that context is briefly addressed. Photoemission measurements from gas-phase alkali halides (CsX, X = F, Cl, Br, I, but also NaI and Cs^0) were performed for comparison, since in these systems each atom is at least partially charged. The electron binding energies measured for CsX (X = F, Cl, Br, I) and aqueous Cs^+ appear to be rather similar; at the level of present theoretical understanding these results are, however, difficult to be interpreted. The analogous anion case was studied for CsI and NaI gas-phase molecules. Again quite similar, $I^-(4d)$ electron binding energies were observed for the aqueous ion and the gas-phase species. Here, further conclusions are hampered since the $I^-(4d)$ ionization energy of gas-phase I^- is unknown.

Another aspect studied, in the context of alkali halide gas-phase measurements, was the $I^-(4d)$ shape resonance near 100 eV. The resonance maximum is found to be at highest energies (ca. 100 eV photon energy) for aqueous iodide. For I_2 and I^+ the maximum is at ca. 90 eV, and even lower for I^0. These data are suggested to point to an increase of the potential barrier height, resulting in a larger delayed onset.

The other important topic regarding photoemission from aqueous salt solution was the structure of solution interfaces. This is a particular challenge for photoemission studies in the range of small information depth, which is the case here. Two different processes were investigated, ion depletion near the solution surface for high-concentration NaI solutions, and the surface segregation of hydrophobic tetrabutylammoiumiodide, But_4NI (but also the smaller tetrapropylammoniumiodide, $Prop_4NI$). The former aspect is related to the question if for high NaI concentration, Na^+ and I^- ions at the solution surface are incompletely

solvated, and also to the question if there is an anion surface excess as has been suggested by several authors (not only for clusters). Neither one was found to be the case based on the present experiments. This conclusion is derived from the constant anion to cation signal ratio as a function of the salt concentration but it is also inferred from the constant aforementioned electron binding energy. However, the present results strongly indicate the existence of a surface depletion layer, as inferred from the sub-linear signal increase of both ion signals for concentrations above 2 m. This structure would in fact be consistent with full-shell solvation keeping the ions away from the liquid/vacuum interface.

The studies of surface-active But_4NI not only confirmed that But_4N^+ segregates at the surface, and that this tendency decreases with the alkyl chain length, it was also confirmed that But_4N^+ surface segregation is favorable for larger co-anions. Using photoemission specifically allows the identification of the completion of the surface monolayer (i.e. the electric double layer composed of *paired* But_4N^+ and I^- ions). The full segregation layer is proposed to coincide with a distinct discontinuity of the iodide signal intensity as a function of the salt concentration. Moreover, the spectral shifts observed for But_4NI solution spectra clearly indicate the importance of molecular surface dipoles and rather disprove earlier interpretations in terms of incomplete ion solvation. Hence, as inferred from the low-energy cutoff of the photoemission spectra the observed apparent binding energy shifts as a function of the salt concentration have to be assigned to a change of the solution work function. Details as to the number and orientation of surface dipoles (i.e. of But_4N^+ and I^- surface density and relative orientation) may be principally assessed by the present technique, however, further experiments would be required for that.

Future experiments will increasingly focus on an optically excited liquid jet, e.g. heading to study the photon-induced dynamics in a solvent environment. Some of the perspectives will be presented in 5.2. Section 6.1 also describes actual preliminary work on this topic.

5.2 Outlook

In the present work it was demonstrated that photoemission may be successfully applied to highly volatile targets which, in combination with synchrotron radiation, allows to directly access electron binding energies of solvated ions, photoionization cross sections, and others. Based on observed spectral shifts and relative photoemission intensities of the ions, various aspects of fundamental processes occurring in aqueous solutions were addressed. With this experience now achieved, one may investigate more complex systems. Obviously, biological molecules are among the interesting systems.

Another experimental challenge is the study of photon-induced processes in the liquid, which opens up for an enormous potential for photoemission of, e.g. optically (transiently) excited species. The field one would like to cover by such two-color two-photon photoemission experiments (2C-2PPE; see section 6.2) is extremely manifold. At this point I only like to address two specific experiments, which on the one hand are in the very context of the present work, and on the other hand, constitute the first test experiments, performed during the most recent beamtime. The first experiment is concerned with the possibility to excite an I^-_{aq} charge-transfer-to-solvent (CTTS) complex by VUV photons ($\sim 50\,\mathrm{eV}$) and to determine the *binding energy* of the solvated electron (e^-_{aq}) in the ground state (see 5.2.1). The second experiment has two parts, the formation and the photodissociation/recombination of an ion complex, I^-_3, in aqueous solution, respectively (see section 5.2.2). The latter study requires time-correlated laser/synchrotron radiation pulses (see sections 6.1 and 6.2). Both subjects will be treated only briefly - it is just an outlook on some potential experiments!!

5.2.1 Charge-Transfer-to-Solvent Absorption and Solvated Electron

Halide ions in aqueous solution exhibit characteristic absorption bands, which correspond to the excitation of an electron into states created by the stabilizing solvent. These are the so called CTTS bands (charge-transfer-to-solvent) referring to an electron being transferred into the solvent. No such bound state exists for the gas-phase species. The situation is depicted schematically in Fig. 5.1, which has been reproduced from Ref. [48]. For I^-, the transition to the lowest CTTS state (Fig. 5.2b) is the promotion of a $5p$ electron into an s-like diffuse orbital. This orbital is delocalized over the first solvation shell, but still centered on the iodine atom. For aqueous iodide, I^-_{aq}, the energy levels relevant for CTTS absorption are

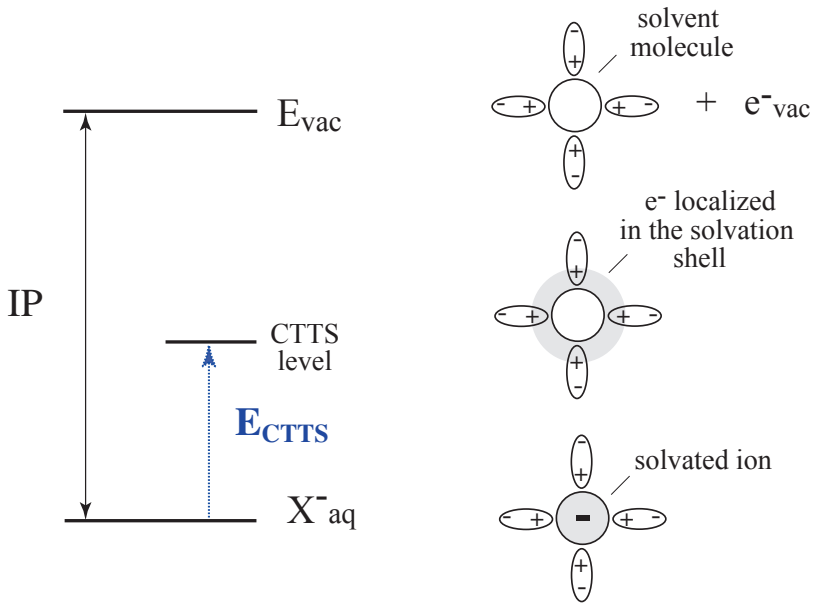

Figure 5.1: *Cartoon of the processes relevant in CTTS state excitation for an aqueous anion together with the corresponding energy levels. IP denotes the threshold ionization energy, and E_{CTTS} is the energy required for excitation of the ground-state aqueous halide ion into the CTTS state. The negative charge distribution is indicated by shadowing. The figure was adapted from Ref. [48].*

shown together with the levels of the resulting trapped electron e^-_{aq} in Fig. 5.2a,b.

Subsequent to CTTS absorption the electron detaches and gets trapped by the solvent within 200 fs. Electron-iodide recombination is observed to take place on ca. 25 ps timescale, but a reasonable fraction of electrons escape (direct) recombination beyond 400 ps [49]. To date, the mechanism for the initial appearance of the trapped electron and the precise nature of the excited state in the parent that leads to its ejection is still poorly understood [49]. The electron may be characterized by intermediate states after formal decay of the CTTS state, before trapping as a ground state solvated electron (e.g. via (e^-)*, known as 'wet' state) [49]. This is the solvated (equilibrated) electron in its ground state, denoted e^-_{aq} or e^-_{eq}.

Notice that the solvated electron may be generated by several other mechanisms as well, e.g. by radiolysis, electrochemistry, or by UV single and multiphoton ionization of water (threshold energy ca. 6 eV) [132]. The proposed structure of the e^-_{aq} in water is a solvent cavity formed by six molecules [133] with a radius of about 2.2 Å [133]. The ground level of the electron in this cavity is a $1s$ state, and the absorption band centered at 720 nm corresponds to transitions to $2p$ levels that are believed to be separated by approximately

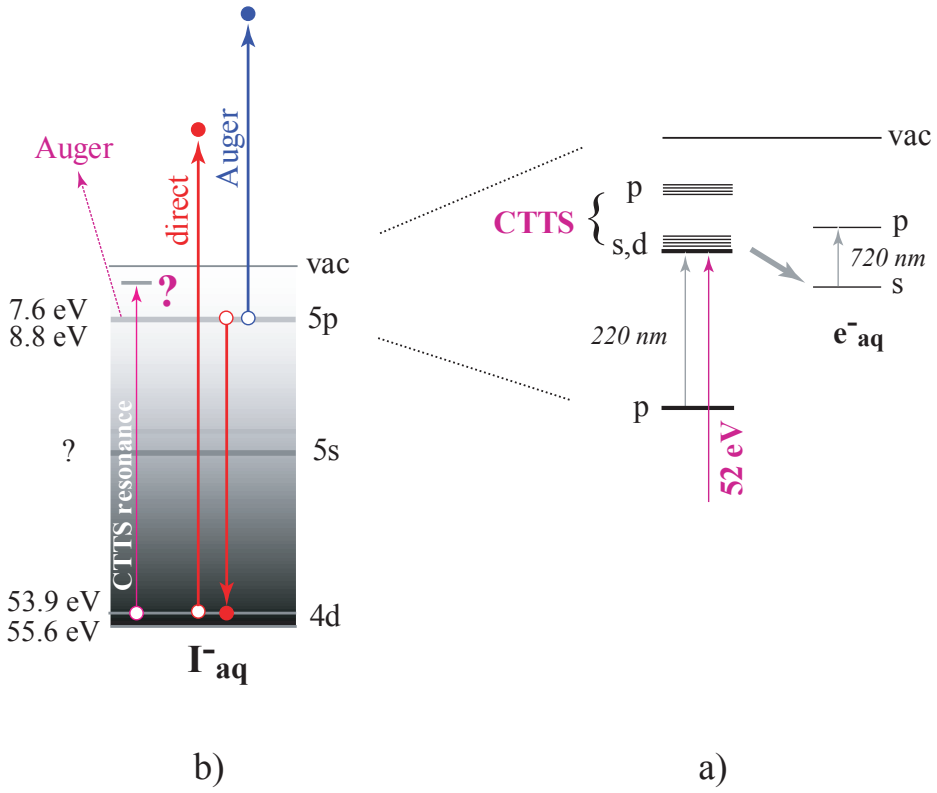

Figure 5.2: *a) Schematic of the relevant transitions for the detachment experiment. The CTTS band of I^-_{aq} is resonantly pumped; the electron is rapidly detached from the CTTS state and the appearance of the trapped electron is probed by transient absorption, or e^-_{aq} provides the basis for studying the dynamics of its excited state e^-_{ex}. b) Schematic level diagram of the proposed 4d-CTTS inner-shell resonance absorption and subsequent Auger decay.*

0.5 eV [134] (see also Fig. 5.2a). Higher excited states form a continuum, approximately 1 eV above the $2p$ level [132, 135]. The lifetime of the solvated electron in its ground state is generally longer than several nanoseconds, depending on the concentration of electron scavengers.

Current studies on the dynamics of the excited solvated electron, e^-_{ex}, make use of the mechanism in Fig. 5.2, i.e. by creating e^-_{aq} via CTTS absorption. This requires three laser pulses [136], the first to excite into the CTTS state, and two (well) delayed pulses, pump and probe, for $e^-_{aq} \rightarrow e^-_{ex}$ excitation and interrogation of the transient state, respectively. From transient absorption measurements the relaxation was found to involve two intermediate states, having a lifetime of 190 fs and 0.9 ps, respectively. The role of solvent relaxation in the excited state is not yet resolved [136].

Interestingly, no report exists yet on the *absolute* binding energy of the ground state hydrated electron e^-_{aq} in bulk water [65]; the present photoemission experiment may have the potential to access this value.

Another interesting point directly related to the CTTS state is the possibility of its excitation from an inner shell, namely from the $I^-(4d)$ level, as motivated in Fig. 5.2b. For photon energies larger than about 56 eV, which is the electron binding energy of $I^-(4d)$, the direct photoemission of $I^-(4d)$ electrons is accompanied by Auger emission involving the iodide $5p$ level (as discussed in section 4.2.2). For photon energies below 56 eV no $5p \rightarrow 4d$ transition occurs, and hence Auger electrons are not generated, unless one of the CTTS states is resonantly excited as depicted in Fig. 5.2a. The cross section for the processes may be low, but more important, the experiment should be better performed in the constant initial state spectroscopy mode, CIS, which uses synchronous scanning of the photon energy and the transmitted electron energy of the analyzer. Preliminary experiments, measuring photoemission spectra from 5 m NaI solution in our standard mode (ramping of electron kinetic energy at given photon energy), for a number of photon energies in the vicinity of 52 eV, have not been conclusive likely due to poor statistics.

5.2.2 I_3^- Complex Formation and its Photodissociation in Aqueous Solution

The molecular structure, reaction dynamics, rates and yields in solution are significantly influenced by solvent environments. The photodissociation and the following recombination of aqueous triiodide is one popular example. Triiodide is formed in solution through the equilibrium reaction:

$$I^- + I_2 \rightleftharpoons I_3^- \,. \tag{5.1}$$

Also larger polyiodide ions may be stable in aqueous solution, their existence, however, is controversially [137].

The molecular properties of the triiodide ion in polar liquids were studied by many techniques in the past, motivated in part by the expected strong coupling between the solute I_3^- electronic structure and the solvent environment [138]. In particular, experiments suggest that the high-symmetry ground-state structure may be broken by the interaction with counter ions or solvent molecules [138].

Other important observations concern the excited-state dynamics of I_3^-. Femtosecond laser flash photolysis studies examined photodissociation and recombination dynamics of

triiodide in water and ethanol [139], however, detailed studies of the solvent effect on the excited states of I_3^- in solution are still far from complete. Photoexcitation near 300 nm [139] or 400 nm [140] leads to the direct formation of diiodide ions in solution within 300 fs [140, 139], according to:

$$I_3^- + h\nu \dashrightarrow I_2^- + I\,. \tag{5.2}$$

UV transient absorption measurements of the photolysis fragments was used to determine the time scales for recombination of the products [139]. The probability and dynamics of caging strongly depends on the choice of the solvent. Three temporal phases of reactant recombination, characterized by time scales of ca. 2 ps, 45 ps, and about 350 ps duration were identified for ethanol solution. The two former time scales were ascribed to the direct recombination of caged fragments (which never escaped the solvent cage) and to the formation of long-living complexes of unknown structure, respectively [139]. The slowest process might be identified with encounters of pairs that have initially escaped the cage. All the paths lead to ground-state I_3^-. As an example, in Fig. 5.3 experimental data from Ref. [141] showing the transient absorption of diiodide following 308 nm photolysis of triiodide in ethanol, is reproduced. The corresponding absorption spectrum of triiodide and the energy diagram

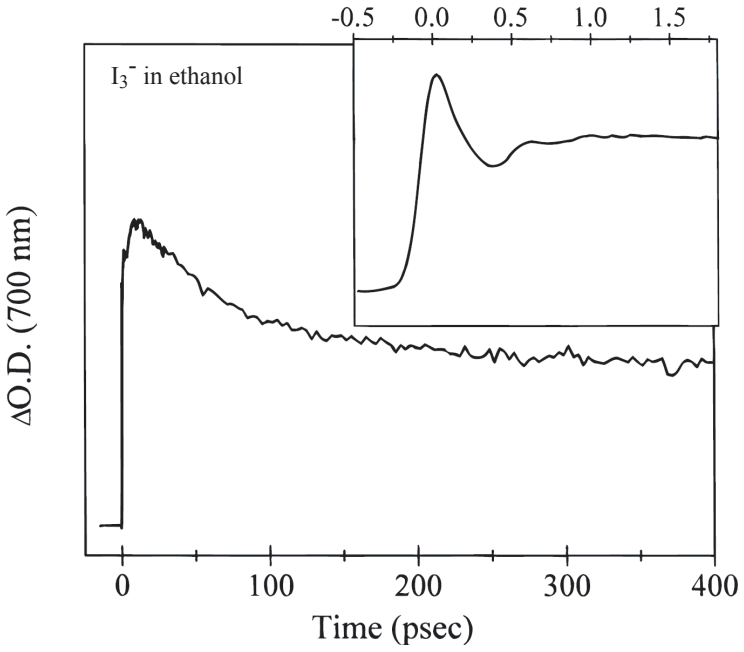

Figure 5.3: *Transient absorption scan at 700 nm following 308 nm photolysis of triiodide in ethanol solution. The inset shows the first 2 ps of probe delay within which spectral modulations due to vibrational coherence in photoproducts is observed [141].*

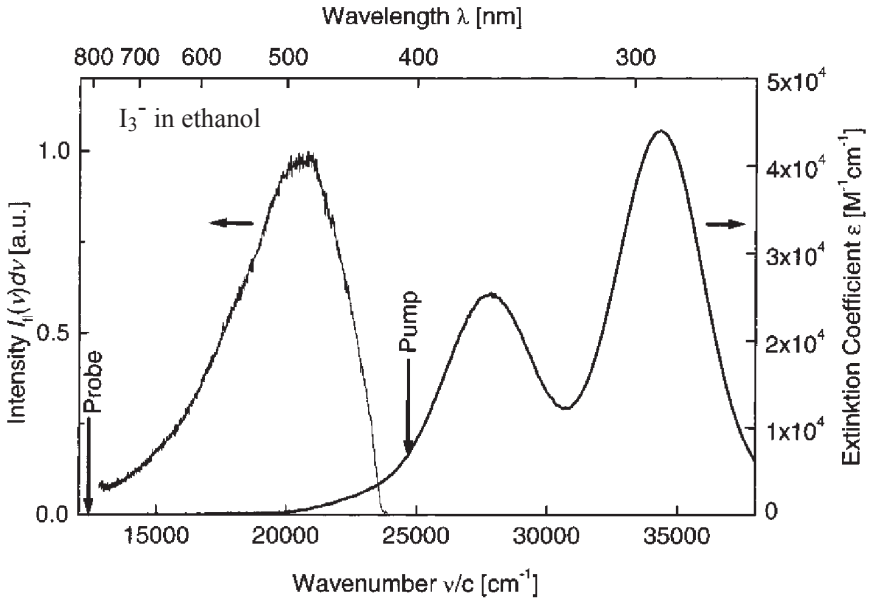

Figure 5.4: *Absorption and emission spectra of triiodide in ethanol [142].*

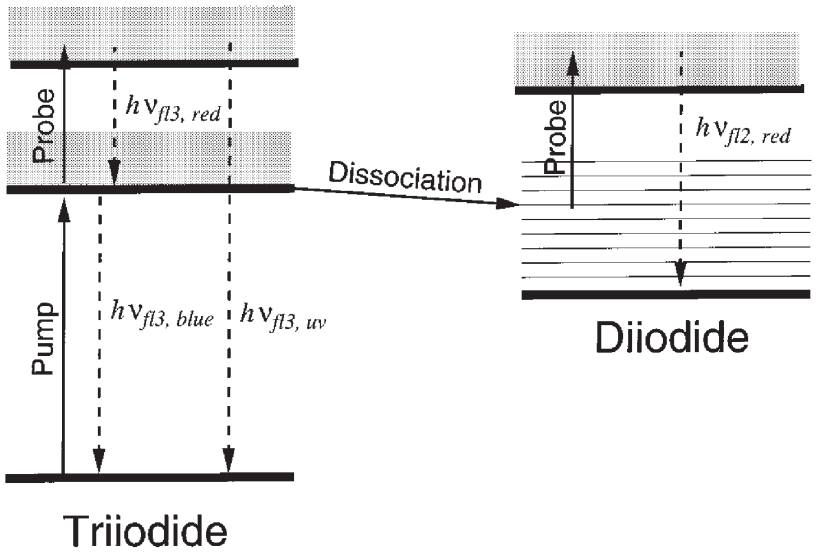

Figure 5.5: *Jabloniski diagram of the photophysics of triiodide. Dissociation continua are represented by shaded areas. Solid arrows stand for absorption processes, dashed arrows stand for fluorescence emission [142].*

containing the relevant transition energies are presented in Fig. 5.4 and Fig. 5.5, respectively, both being reproduced from Ref. [142].

The long-lifetime component of one of the recombination processes (Fig. 5.3) makes the I_3^- system particularly interesting for 2C-2PPE experiments using combined laser and synchrotron radiation pulses (with a time resolution of about 30 ps; see Appendix, 6.1). Clearly, following the temporal evolution of the photo-products by changing the time delay of the laser pump with respect to the synchrotron radiation probe pulse is a major challenge.